RP Materials: Proceedings
Vol. 3, Part 1 (2023) pp. 17–21
e-ISSN: 2583-8342

RESEARCH PLATEAU PUBLISHERS

Cite this article: A. Thomas, S. Thomas, Effect of Sb addition on physical and optical properties of ternary Ge-Se-Te glasses, *RP Materials: Proceedings* Vol. 3, Part 2 (2024) pp. 17–21.

Original Research Article

Effect of Sb addition on physical and optical properties of ternary Ge-Se-Te glasses

Anila Thomas*, Sheenu Thomas
International School of Photonics, Cochin University of Science and Technology, Kochi, 682022, India
*Corresponding author, E-mail: anilathomas241@gmail.com

****Selection and Peer-Review under responsibility of the Scientific Committee of the International Conference on Composite Materials for Environment Protection & Remediation 2024 (ICCMEPR 2024).**

ARTICLE HISTORY
Received: 2 July 2024
Revised: 12 August 2024
Accepted: 14 August 2024
Published online: 19 August 2024

KEYWORDS
Chalcogenide glasses; Co-ordination number; Optical bandgap; Transition temperature.

ABSTRACT
Chalcogenide glasses are amorphous solids that include at least one of the chalcogen elements (S/Se/Te). Our work investigates the changes in physical and optical properties of the GeSeTe glass matrix when Te is substituted with Sb. The bulk chalcogenide glass is prepared by the conventional melt quench method. X-ray diffraction (XRD) is employed to determine the amorphous nature of bulk samples. The ratio of compositional elements is verified using Energy-Dispersive X-ray spectroscopy (EDS). Diffuse reflectance spectroscopy (DRS) is employed to assess the optical bandgap arising from indirect electronic transitions. Its value changes with the incorporation of Sb as the fourth element. Differential scanning calorimetry (DSC) studies demonstrate that the addition of Sb leads to a higher transition temperature, enhancing the cross-linking and consequently the rigidity of the glass. IR transparency of these glasses is observable in the FT-IR spectrum except for some impurity absorption. These glasses prove to be good optoelectronic materials for the fabrication of photonic structures.

1. Introduction

Chalcogenide glasses (ChGs) are a type of non-oxide glasses that exhibit infrared (IR) transmission. These glasses are composed primarily of elements from Group XIV, XV, and XVI in the periodic table, excluding oxygen. Their ability to transmit infrared light and their customizable optical and physical characteristics are attributed to their wide-ranging propensity for glass formation. A diverse range of compositions in glass-forming systems, combined with excellent resistance to crystallization, produce glasses that possess optical characteristics like nonlinearity, photosensitivity, and transparency to infrared light. These properties can be finely tuned to optimize their performance for photonic applications [1]. Introducing additional dopants like As, Ge, Sb, Bi, Cd, etc. into this material enhances its desired properties while mitigating its limitations. For instance, Ge doping improves thermal stability and expands the glass-forming range, while also reducing aging effects [2]. These dopants interact with selenium chains, modifying bonds. Similarly, Sb dopants, like Ge, improve thermal stability and play a role in modifying the interactions between positive and negative valence pairs [3].

A comprehensive grasp of Ge-Sb-Se, Ge-Se-Te and Ge-Sb-Te systems and their relevance to Ge-Se-Sb-Te (GSST) systems would provide a detailed overview of the unique characteristics of GSST materials. Studies highlight that Ge-Sb-Se materials show efficient transmission with minimal loss, strong thermal stability and excellent transparency in the infrared range [4, 5]. On the other hand, Ge-Sb-Te (GST) materials are notable for their swift transition from amorphous to crystalline states. This capability is highly beneficial for applications like phase change memory (PCM) due to the distinct contrast in optical reflectivity and electrical resistance between the amorphous and crystalline states [6]. The studies on GeSeTe glasses highlight the extensive IR transparency extending upto far IR regime and low impurity absorption, even though these glasses are prone to devitrification due to the presence of tellurium [7, 8]. Therefore the GSST glass family is expected to exhibit the superior properties of these glass families.

Since 1978, researchers have conducted numerous studies focusing on the physical, thermodynamic and optical properties of glassy GSST alloys. Surinach et al. [9] investigated aspects such as glass formation and crystallization in $GeSe_2$-Sb_2Te_3 alloys. Bartak et al. [10] investigated additional bulk material properties such as crystal growth and viscosity in $Ge_2Sb_2Se_{5-x}Te_x$ glasses. Furthermore, Hassanien et al. [2, 11] investigated and analyzed a range of physical properties such as molar mass, molar volume, atomic density, excess volume, free volume percentage, packing density, number of valence electrons, polaron radius, and interatomic separation distance. They investigated the variation of the physical characteristics in $Ge_{15-x}Si_xSe_{50}Te_{35}$ bulk samples by substituting Ge with Sb. Sb enhances the optical characteristics of Ge-Se-Te alloys by reducing the optical band-gap energy, Eg. Therefore, the inclusion of Sb offers numerous benefits when incorporated into chalcogenide alloys [12]. Hence there are more rooms to explore the application of GSST chalcogenide glasses.

2. Materials and methods

2.1 Materials

The raw materials for preparing chalcogenide glasses were pure Ge, Se, Te and Sb powders (5N purity) bought from Sigma Aldrich. Quartz tubes of 1 metre length is made into many ampoules of lesser length for loading the chemicals into it.

2.2 Methods

The selected composition of glasses, $Ge_{20}Se_{60}Te_{20-x}Sb_x$ (x = 0, 5, 10, 15) were prepared by the conventional method of melt quenching. Pure Ge, Se, Te, and Sb of appropriate weight percentage were loaded into quartz ampoules, which can withstand temperature upto 1200°C and are not damaged by the thermal shock on sudden cooling. It is then sealed under vacuum (10^{-3} mbar) to avoid the chances of hydrolysis and oxidation. The samples are melted using a rocking and rotating furnace. During heating, the furnace was rocked and rotated at regular intervals to ensure the homogeneity of the mixture. The temperature was increased at a heating rate of 3 – 4°C/min up to 800°C then slowly increased at the rate of 1 - 2°C/min up to 1050°C for 48 hours and quenched in ice-cooled water. It was then etched in hydrofluoric acid and the samples were taken out. Various characterizations were done after grinding the samples into fine powder using mortar and pestle.

The compositions were chosen in such a way that they are in glass forming region and the average coordination number <m> was between 2.4 and 2.7. The Philips and Thorpe model predicts that a glass network with a low average co-ordination number <m> results in a 'floppy' network with small isolated rigid areas. When <m> reaches 2.4, the network transforms into a stiff glassy structure with small isolated floppy parts, which is known as 'amorphous solid'. These <m> values are essential for converting 2-D chain arrangements to 3-D network architectures [13]

$$< m >= \frac{\alpha N_{Ge} + \beta N_{Se} + \gamma N_{Te}}{\alpha + \beta + \gamma} \quad (1)$$

where α, β, γ are the atomic percentage of Ge, Se and Te and N represents their respective co-ordination number.

2.3 Characterizations

XRD measurements (powder XRD) were performed using Bruker D8 Advance X-ray powder diffractometer (Cu-K_α, λ = 1.5406 Å). Jeol 6390LA/ OXFORD XMX N was used for EDS analysis. Optical characterizations of finely powdered bulk samples were examined using Jasco V 770 UV/VIS/NIR spectrophotometer for acquiring solid-state spectrum in diffuse reflectance mode (DRS). This spectrophotometer operates over the range of 200 nm to 3000 nm with DRS integrating sphere diameter of 150 mm and angle of incidence 8°. The Fourier Transform Infrared (FT-IR) spectra were recorded using the Thermo Nicolet iS50 FTIR spectrometer over the wavelength range from 400 cm^{-1} to 4000 cm^{-1}. The glass transition temperature (T_g), an important characteristic of the glass, was investigated using a Netzsch DSC 204 F1 Heat flux DSC instrument. The samples were heated at a rate of 10°C per minute, progressing from 50°C to 300°C under a nitrogen (N_2) atmosphere.

3. Results and discussion

3.1 X-ray diffraction (XRD)

XRD is a technique used to analyse amorphous nature of materials. XRD patterns reveal a broad scattering halo that confirms structural disorder in the prepared glassy alloys [14]. The non-crystalline XRD profiles exhibit prominent stepped humps at two specific angular ranges. The first and more pronounced hump appears between 2θ = 15 to 35 degrees, while a smaller, less intense hump is observed from 45 to 55 degrees. These features are attributed to the amorphous nature of the glass substrate used in the study [15, 16].

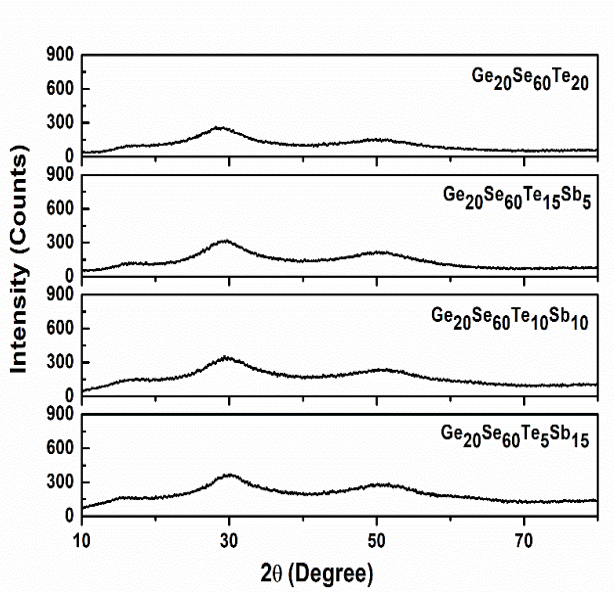

Figure 1: X-ray diffraction pattern of $Ge_{20}Se_{60}Te_{20-x}Sb_x$ (x = 0, 5, 10, 15) glass compositions.

3.2 Energy-dispersive X-ray spectroscopy (EDS)

EDS is a technique mostly used for the qualitative and semi-quantitative analysis of the sample. The elemental composition of these samples were confirmed to be similar to that of nominal composition from Figure 2. The proposed composition and actual composition is given in Table 1.

3.3 Diffuse reflectance spectroscopy (DRS)

The suitability of these materials for various applications is evaluated based on their unique characteristic, such as the bandgap energy (E_g). When light interacts with the powdered sample, a portion is reflected from the surface, while the rest penetrates inside and disperses. The absorption of light at specific wavelengths and the measurement of the scattered reflected light yield the diffuse reflectance spectrum [17, 18]. A graph is plotted where energy (E) is along the x-axis, and $[F(R) \times E]^{0.5}$along the y-axis, where $F(R)$, known as the Kubelka-Munk function, is given by

$$F(R) = \frac{k}{s} = \frac{(1-R)^2}{2R} \quad (2)$$

Here k represents the absorption coefficient, R denotes the absolute reflectance, and s indicates the scattering coefficient.

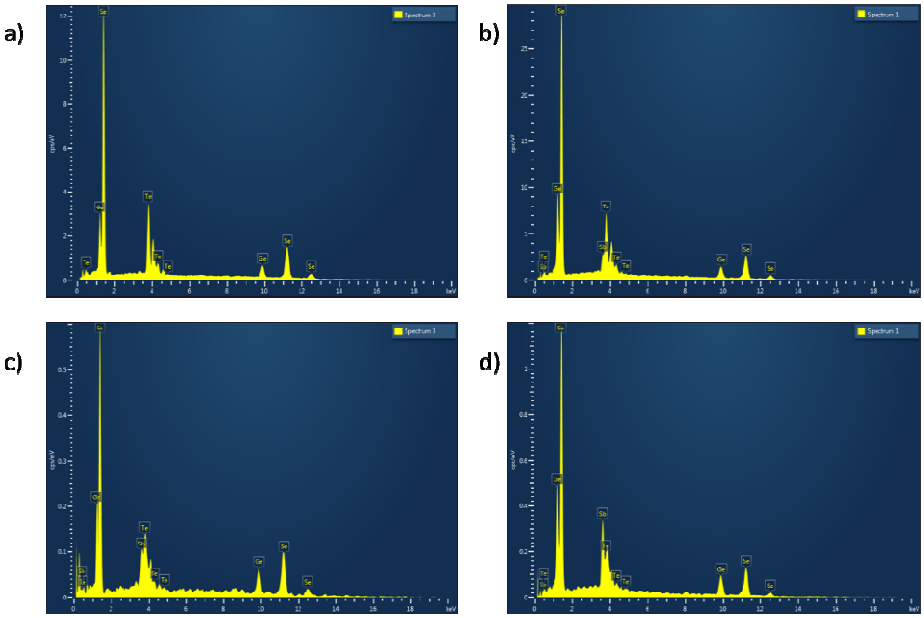

Figure 2: EDS spectrum of (a) $Ge_{20}Se_{60}Te_{20,}$ (b) $Ge_{20}Se_{60}Te_{15}Sb_5$, (c) $Ge_{20}Se_{60}Te_{10}Sb_{10}$, (d) $Ge_{20}Se_{60}Te_5Sb_{15}$ bulk powder samples.

Table 1: Experimental composition obtained from EDS measurement

Material	Target Composition At%				Actual Composition At%			
	Ge	Se	Te	Sb	Ge	Se	Te	Sb
$Ge_{20}Se_{60}Te_{20}$	20	60	20	0	17.1	60.42	22.5	0
$Ge_{20}Se_{60}Te_{15}Sb_5$	20	60	15	5	20.9	59.21	15.45	4.47
$Ge_{20}Se_{60}Te_{10}Sb_{10}$	20	60	10	10	16.86	60.8	11	11.33
$Ge_{20}Se_{60}Te_5Sb_{15}$	20	60	5	15	19.66	57.07	5.47	17.82

By extrapolating the linear portion of the graph to $k = 0$, we can estimate the bandgap (E_g) of the material. The reflectance spectrum of the glasses of various compositions in Figure 3 shows that there is an increase in reflectance as Sb content increases and also there is a shift in the band tail to lower wavelength region. As the amount of Sb increases at the expense of Te, there is a reduction in the concentration of Te–Te (33 kcal/mol) and Se–Se (44.04 kcal/mol) bonds, while Se–Sb (43.98 kcal/mol) and Sb–Te (31.65 kcal/mol) bonds become more prevalent. This shift results in an overall higher average bond energy within the glass matrix, which can be effectively understood through the covalent bond model. This change is a potential explanation for the observed increase in the bandgap [2].

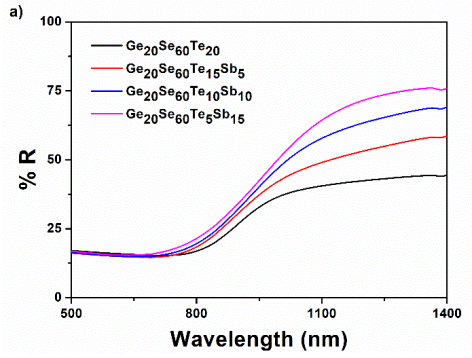

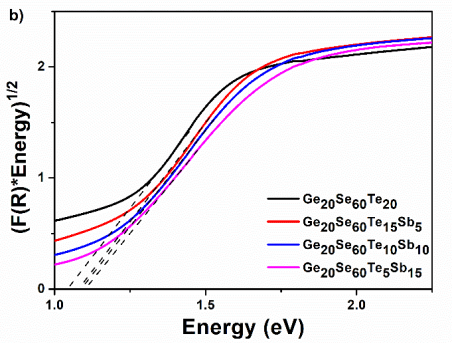

Figure 3: (a) DRS spectrum of $Ge_{20}Se_{60}Te_{20-x}Sb_x$ ($x = 0, 5, 10, 15$) powder samples;
(b) shows the optical bandgap determined using Kubelka and Munk function.

Table 2: Variation of coordination number, optical bandgap and transition temperature with increase in Sb content

Sample	<m>	E_g (eV)	T_g (°C)
$Ge_{20}Se_{60}Te_{20}$	2.4	1.04	105.4
$Ge_{20}Se_{60}Te_{15}Sb_5$	2.45	1.08	163.0
$Ge_{20}Se_{60}Te_{10}Sb_{10}$	2.5	1.09	197.0
$Ge_{20}Se_{60}Te_5Sb_{15}$	2.55	1.10	251.2

3.4 Differential scanning calorimetry (DSC)

DSC quantifies the heat energy exchanged by a system relative to temperature changes. In DSC, glass powder undergoes heating within a sample pan, and the heat exchanged is compared with an adjacent empty reference pan. This comparison reveals any phase transitions occurring within the sample, detected by differences in heat flow between the two pans [19]. Glass transition temperature, T_g, the temperature at which transition occurs from rigid solid to supercooled liquid state, is denoted as the inflection point of the DSC thermogram [20]. As the atomic percentage of Sb is increased in the Ge-Se-Te-Sb glass system, Sb tends to preferentially bond with Se because the bond energy of Sb-Se exceeds that of Sb-Te. Consequently, the proportion of Se-Se bonds decreases, while the number of Sb-Se bonds increases with higher Sb content [21]. The addition of Sb which is more coordinated than Te, increases the networking within the glass matrix resulting in the increase in transition temperature. In Figure 4, the increase in transition temperature is observable with the increase in the percentage of Sb added.

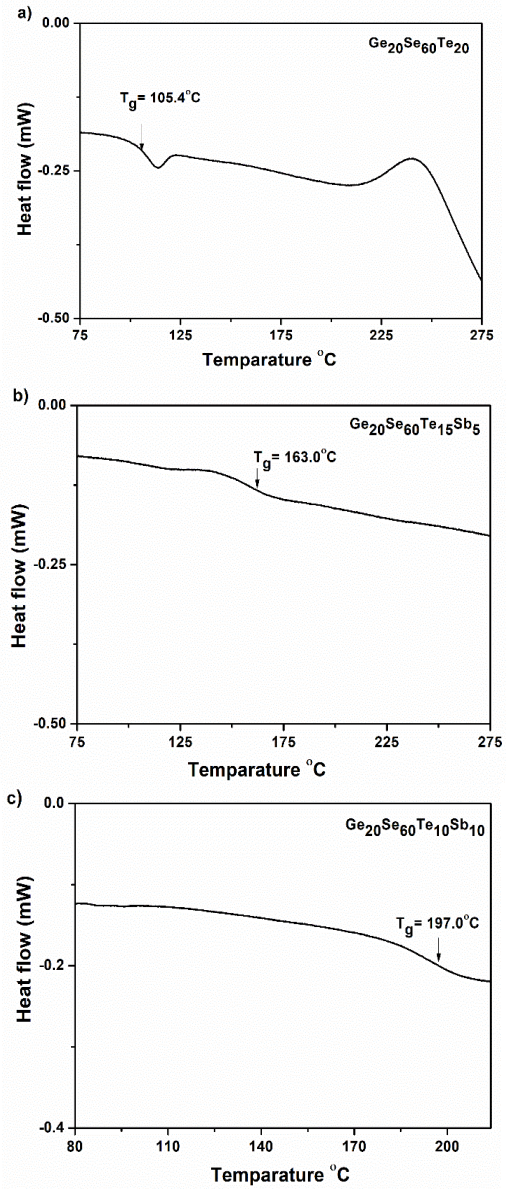

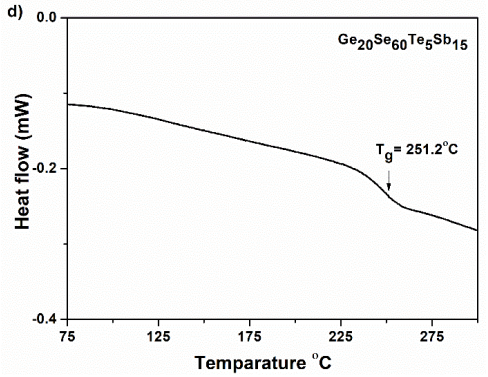

Figure 4: DSC Thermogram of (a) $Ge_{20}Se_{60}Te_{20}$; (b) $Ge_{20}Se_{60}Te_{15}Sb_5$; (c) $Ge_{20}Se_{60}Te_{10}Sb_{10}$; (d) $Ge_{20}Se_{60}Te_5Sb_{15}$ bulk powder samples.

3.5 Fourier transform infrared spectroscopy (FTIR)

FTIR provides information about the vibrational spectra of different molecular species present in a material. FTIR data cannot provide structural information on chalcogenide glasses, instead, it is used to identify the impurities present in the sample. All the compositions exhibit high infrared transparency, though they may include some impurity absorption bands. In the FTIR spectra recorded the primary source of impurity absorption is hydrogen, with absorption bands at 3236.36 cm^{-1}, 3507.4 cm^{-1}, and 3587.4 cm^{-1} corresponding to molecular H_2O, while the band at 3470 cm^{-1} is attributed to OH groups attached to the glass network [22,23]. In our samples, these two bands merge to form a broad peak around 3470 cm^{-1}. The absorption peak at 1637.2 cm^{-1} indicates H-O-H scissor bending. Additionally, a small absorption dip observed at 2853.6 cm^{-1} and 2923.07 cm^{-1} is characteristic of the C-H bond [24].

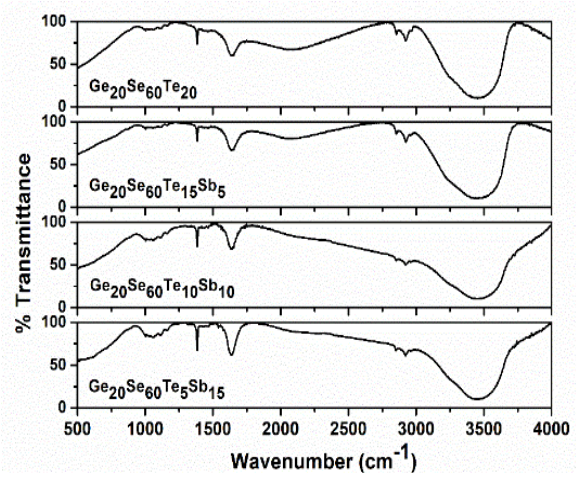

Figure 5: FTIR spectrum of $Ge_{20}Se_{60}Te_{20-x}Sb_x$ (x = 0, 5, 10, 15) glass compositions.

5. Conclusions

$Ge_{20}Se_{60}Te_{20-x}Sb_x$ (x = 0, 5, 10, 15) glasses were synthesized by melt quench method. XRD pattern confirmed the amorphous nature and FTIR spectrum showed that these glasses were IR transparent. EDS analysis ensured that the glasses were similar to nominal composition. Increase in optical band gap was observed from diffuse reflectance

spectrum. There was an increase in T_g considerably with the addition of Sb because higher co-ordination of Sb increases network of bonds. Studies prove the tunability of physical and optical properties such as average co-ordination, E_g and T_g with addition of Sb addition, which can be exploited for various photonic applications.

Acknowledgements

The authors are thankful to Cochin University of Science and Technology (CUSAT) for providing support of Research fellowship and facilities for the research work and SAIF-STIC for XRD, EDS, DSC and FTIR analysis.

References

[1] B.J. Eggleton, B. Luther-Davies, K. Richardson, Chalcogenide photonics, *Nat. Photon.* **5** (2011) 141-148.

[2] A.S. Hassanien, I. Sharma, A.A. Akl, Physical and optical properties of a-Ge-Sb-Se-Te bulk and film samples: Refractive index and its association with electronic polarizability of thermally evaporated a-$Ge_{15-x}Sb_xSe_{50}Te_{35}$ thin-films, *J. Non-Cryst. Sol.* **531** (2020) 119853.

[3] S. Sharda, N. Sharma, P. Sharma, V. Sharma, Physical analysis of structural transformation in Ge-incorporated a-Sb_xSe_{100-x} system, *Def. Diff. Forum*. **316** (2011) 45-53.

[4] N. Sharma, S. Sharda, V. Sharma, P. Sharma, Far-infrared investigation of ternary Ge–Se–Sb and quaternary Ge–Se–Sb–Te chalcogenide glasses, *J. Non-Cryst. Sol.* **375** (2013) 114-118.

[5] W.H. Wei, L. Fang, X. Shen, R.P. Wang, Crystallization kinetics and thermal stability in Ge–Sb–Se glasses, *Phys. Stat. Sol. (b)* **250** (2013) 59-64.

[6] F. Bedeschi, R. Bez, C. Boffino, E. Bonizzoni, E.C. Buda, G. Casagrande, M. Tosi, 4-Mb MOSFET-selected/spl mu/trench phase-change memory experimental chip, *IEEE J. Sol. Stat. Cir.* **40** (2005) 1557-1565.

[7] J.A. Muir, R.J. Cashman, GeSeTe—A new infrared-transmitting chalcogenide glass, *J. Opt. Soc. Am. A* **57** (1967) 1-3.

[8] P. Sharma, S. Katyal, Effect of tellurium addition on the physical properties of germanium selenide glassy semiconductors, *Physica B: Cond. Mat.* **403** (2008) 3667-3671.

[9] S. Suriñach, M.D. Baro, M.T. Clavaguera-Mora, N. Clavaguera, Thermodynamic aspects of glass-formation and crystallization in the $GeSe_2$-S_2Te_3 system, *Fluid Phase Equilibria* **20** (1985) 341-346.

[10] J. Barták, P. Koštál, J. Málek, Analysis of crystal growth and viscosity in Ge-Sb-Se-Te undercooled melts, *J. Non-Cryst. Sol.* **505** (2019) 1-8.

[11] V. Trnovcová, T. Pazurová, T. Šrámková, D. Lezal, Optimizing of multicomponent seleno-telluride glasses for optical fibers applied to power transmission at 10.6 μm, *J. Non Cryst. Sol.* **90** (1987) 561-564.

[12] A. Kaistha, V. Modgil, V.S. Rangra, Structural characterization and compositional dependence of optical properties of $Ge_{16}Se_{52}Te_{32-x}Sb_x$ (x = 0, 2, 4, 6, 8) glassy alloys, *J. Electron. Mater.* **44** (2015) 4747-4753.

[13] Z.G. Ivanova, V. Pamukchieva, M. Vlček, On the structural phase transformations in $Ge_xSb_{40-x}Se_{60}$ glasses, *J. Non-Cryst. Sol.* **293** (2001) 580-585.

[14] S. Mishra, P. Lohia, D.K. Dwivedi, Structural and optical properties of $(Ge_{11.5}Se_{67.5}Te_{12.5})_{100-x}Sb_x$ ($0 \leq x \leq 30$) chalcogenide glasses: A material for IR devices, *Infr. Phys. Technol.* **100** (2019) 109-116.

[15] S.A. Fayek, M. El-Ocker, A.S. Hassanien, Optical and electrical properties of $Ge_{10+x}Se_{40}Te_{50-x}$ thin film, *J. Mater. Res.* **16** (2001) 1549-1553.

[16] A.S. Hassanien, A.A. Akl, Optical characteristics of iron oxide thin films prepared by spray pyrolysis technique at different substrate temperatures, *Appl. Phys. A* **124** (2018) 752.

[17] P. Kubelka, New contributions to the optics of intensely light-scattering materials, Part I. *J. Opt. Soc. Am. A* **38** (1948) 448-457.

[18] P. Kubelka, F. Munk, An article on optics of paint layers, *Z. Tech. Phys*. **12** (1931) 259-274.

[19] A. Jean Luc, Z. Xianghua, *Chalcogenide glasses*, Woodhead Publishing Limited, UK (2014).

[20] M. Yamane, A. Yoshiyuki, *Glasses for Photonics*, Cambridge University Press, New York (2000).

[21] S. Gupta, A. Agarwal, M. Saxena, Study of crystallization kinetics of some tex $(Bi_2Se_3)_{1-x}$ glassy alloys, *Adv. Appl. Sci. Res.* **2** (2011) 49-57.

[22] K. Reichelt, X. Jiang, The preparation of thin films by physical vapour deposition methods, *Thin Sol. Films* **191** (1990) 91-126.

[23] D.S. Ma, P.S. Danielson, C.T. Moynihan, Bulk and impurity infrared absorption in $0.5As_2Se_3$ 0.5 $GeSe_2$ glass, *J. Non-Cryst. Sol.* **37** (1980) 181-190.

[24] M.E. Fortună, E. Ungureanu, C.D. Jitareanu, Calcium carbonate–carboxymethyl chitosan hybrid materials, *Materials* **14** (2021) 3336.